



Nano-Li₄Ti₅O₁₂ with high rate performance synthesized by a glycerol assisted hydrothermal method

Wenli Zhang ^a, Jinfeng Li ^a, Yibiao Guan ^b, Yi Jin ^b, Wentao Zhu ^a, Xun Guo ^a, Xinping Qiu ^{a,*}

^a Key Laboratory of Organic Optoelectronics and Molecular Engineering, Department of Chemistry, Tsinghua University, Beijing 100084, China

^b China Electric Power Research Institute, Beijing 100192, China



HIGHLIGHTS

- We report a glycerol assisted approach to obtain pure nano-Li₄Ti₅O₁₂.
- An accurate Ti:Li ratio should be adopted in order to obtain pure Li₄Ti₅O₁₂.
- The introduction of glycerol plays an important role.
- Glycerol assisted sample exhibits excellent rate and good cycling performance.

ARTICLE INFO

Article history:

Received 9 April 2013

Received in revised form

3 June 2013

Accepted 4 June 2013

Available online 20 June 2013

Keywords:

Glycerol assisted

Hydrothermal method

Lithium ion batteries

Lithium titanate

ABSTRACT

Here we report a facile approach to synthesize pure nano-Li₄Ti₅O₁₂ by a glycerol assisted hydrothermal process and subsequent thermal treatment. During the hydrothermal process, the introduction of glycerol helps to control the morphologies of products and significantly improve the electrochemical performance of Li₄Ti₅O₁₂ as an anode material. On the other hand, an accurate Ti:Li ratio is controlled in order to obtain pure Li₄Ti₅O₁₂ since the Ti:Li ratio of starting materials sensitively impacts the final composition of product. X-ray diffraction, thermogravimetric-differential scanning calorimetry, field-emission scanning electron microscopy and transmission electron microscopy are used to characterize their structures and morphologies. The glycerol assisted sample annealed at 500 °C can retain a discharge capacity of 154 mAh g⁻¹ after 500 cycles at 5 C and deliver a high discharge capacity of 155 mAh g⁻¹ at 20 C. The excellent cycling and rate performance can be attributed to the minor particle size, lower charge-transfer resistance (15.8 Ω) and larger lithium ion diffusion coefficient (4.32 × 10⁻¹¹ cm² s⁻¹).

© 2013 Elsevier B.V. All rights reserved.

1. Introduction

Recently, lithium ion batteries (LIBs) have attracted great attention as the potential candidates for hybrid electric vehicles (HEVs) and electric vehicles (EVs) due to their high energy density and long cycle life [1–4]. But to achieve extensive application, excellent kinetic performance and high safety are two crucial factors which are highly concerned for LIBs materials [5–7]. Spinel Li₄Ti₅O₁₂ is regarded as one of the most promising anode materials due to its unique properties. Compared with graphite, Li₄Ti₅O₁₂ has a flat voltage plateau at approximately 1.55 V versus Li⁺/Li, which is above the reduction potential of electrolyte solvents [8,9]. Therefore it is effective to avoid the formation of the solid electrolyte interface (SEI) passive layer and the emergence of the lithium dendrite on

the surface of Li₄Ti₅O₁₂ within the operating voltage range. Furthermore, known as a zero-strain insertion material, spinel Li₄Ti₅O₁₂ benefits from its negligible lattice change during the Li-ion insertion/desorption process [10,11]. Hence Li₄Ti₅O₁₂ can exhibit a long cycle life, promising high rate capabilities and lower security risks.

Although Li₄Ti₅O₁₂ holds some exciting advantages, its inherent low electronic conductivity (<10⁻⁹ S cm⁻¹) leads to poor high rate performance [12,13]. Interestingly, nanostructured Li₄Ti₅O₁₂ often shows good rate ability, for it leads to improved kinetic performance by reducing the transport path lengths of lithium ions and electrons. Kavan et al. concluded that the effective diffusion distance was closely related with the rate ability and the particle size should be less than 100 nm to achieve a high rate (≈ 200 C) at a diffusion coefficient of 10⁻¹² cm² s⁻¹ for electrode materials [14]. Various nanostructured Li₄Ti₅O₁₂ with excellent rate performance have been synthesized, such as hollow microsphere [15], mesoporous microsphere [16], sawtooth-like nanosheets [17] and

* Corresponding author. Tel./fax: +86 10 62794234.

E-mail addresses: qiuxp@mail.tsinghua.edu.cn, 823406675@qq.com (X. Qiu).

nanotubes [18]. Another tricky problem needs to be solved is how to obtain really pure materials. For multiple synthesis methods including solid reaction [19,20], sol–gel route [21,22], hydrothermal process [23,24] and molten salt method [25,26], it is found that impurity phases like TiO_2 and Li_2TiO_3 are easily to appear during the synthesis of $\text{Li}_4\text{Ti}_5\text{O}_{12}$. When TiO_2 and lithium salts are used as the reactants of final step, it often needs a long time and relatively high temperature to obtain pure $\text{Li}_4\text{Ti}_5\text{O}_{12}$, even though using different types of nanosized TiO_2 [14,27,28]. The main reason may be the Ti:Li ratio gradually deviates from the desired proportion under a prolonged heating time at high temperature. The most obvious phenomenon is the loss of the lithium salts during the heat treat process. In addition, most of titanium salts are not stable enough in air or solutions which will also impact the accurate proportion of reactants. Therefore how to obtain pure nano- $\text{Li}_4\text{Ti}_5\text{O}_{12}$ with excellent rate performance is a big challenge.

Glycerol has been used to assist the formation of various inorganic nano-materials in hydrothermal synthesis, because of its unique solvent properties and excellent ability to form hydrogen bonds with other compounds [29–31]. During the synthesis process, it mainly acts as the shape-controller, reducing agent and hydrolyzation inhibitor. In this work, we report a soft synthetic route to obtain nano- $\text{Li}_4\text{Ti}_5\text{O}_{12}$ by a glycerol assisted hydrothermal process followed with a short post-annealing procedure. $\text{Ti}(\text{SO}_4)_2$ is selected as the titanium source due to its good solubility and stability in solution. During the hydrothermal process, glycerol is added as a modifier to assist the dispersion of starting materials, which can help to control the morphology of $\text{Li}_4\text{Ti}_5\text{O}_{12}$ and improve the electrochemical performance. Meanwhile, an accurate Ti:Li ratio is controlled in order to obtain pure $\text{Li}_4\text{Ti}_5\text{O}_{12}$ since the Ti:Li ratio of starting materials sensitively impacts the final composition of product. The as-prepared nano- $\text{Li}_4\text{Ti}_5\text{O}_{12}$ displays a cubic morphology and exhibits high rate capacity and good cycling performance.

2. Experimental section

2.1. Synthesis of spinel $\text{Li}_4\text{Ti}_5\text{O}_{12}$

Spinel $\text{Li}_4\text{Ti}_5\text{O}_{12}$ nanoparticles were prepared by a hydrothermal process. All of the chemicals were of analytical grade and used without further purification. In a typical procedure, deionized water (15 mL) and glycerol (5 mL) were mixed together under vigorous stirring. After stirring for 10 min, $\text{Ti}(\text{SO}_4)_2$ (4 mmol) was dissolved in the previous solution to obtain solution A. At the same time, a fixed amount of $\text{LiOH} \cdot \text{H}_2\text{O}$ was dissolved in deionized water (20 mL) to obtain solution B. In order to study the impact of adding different amounts of lithium salts, three Ti:Li mole ratio were applied in this experiment (Ti:Li = 1:4.5075, 1:4.5125 and 1:4.5175). After stirring for 30 min, solution B was added stepwise into solution A. During the dropping procedure, white gelatinous precipitate appeared in the mixed solution. With the further addition of solution B, the mixture turned into clear solution in the end. Then the obtained clear solution was stirred for another half an hour, followed by a 30 min's supersonic treatment. After that the solution was transferred into a 50 mL Teflon-lined stainless autoclave and maintained at 200 °C for 8 h. The resulting precipitate was washed several times with deionized water to remove the adsorbed Li_2SO_4 and glycerol. After washing, the product was centrifuged and dried at 80 °C in an oven. Finally, the white powder was calcined at a certain temperature (500 °C, 600 °C, 700 °C) for 5 h in air to obtain spinel $\text{Li}_4\text{Ti}_5\text{O}_{12}$. For simple, the as-prepared glycerol assisted samples annealed at different temperature are abbreviated to G-500, G-600 and G-700, respectively. A sample without glycerol annealed at 500 °C (S-500) was also prepared via the same process but substituting the 5 mL glycerol for deionized water.

2.2. Structural and physical characterization

The crystal structure of as-prepared samples was characterized by X-ray diffraction (XRD, Bruker D8 advance), using a Cu-K α radiation source ($\lambda = 1.5406 \text{ \AA}$). The diffraction data were collected at room temperature by step-scanning over the angular range of 10–80°. Microstructure and morphologies were observed on scanning electron microscopy (SEM, Hitachi S-4500), transmission electron microscopy (TEM, JEOL JEM-2011) and high-resolution transmission electron microscopy (HRTEM, JEM-2011F). The specific surface area of prepared $\text{Li}_4\text{Ti}_5\text{O}_{12}$ was determined by Brunauer–Emmett–Teller (BET) measurements using a NOVA 1000e surface area analyzer. The thermal gravimetric-differential scanning calorimetry (TG-DSC) analysis was performed using Universal V5.3C 2050 instrument from room temperature to 900 °C with a scanning rate of 10 °C min $^{-1}$ under air atmosphere.

2.3. Electrochemical characterization

CR2032 coin-type cells were assembled in an argon-filled glove box (German, M. Braun Co., $[\text{O}_2] < 1 \text{ ppm}$, $[\text{H}_2\text{O}] < 1 \text{ ppm}$). The cathode electrode was prepared by mixing the $\text{Li}_4\text{Ti}_5\text{O}_{12}$ powder, carbon black and polyvinylidene fluoride with a weight ratio of 8:1:1 in N-methyl pyrrolidinone. The mixture was pasted on pure Cu foil and dried under vacuum at 100 °C for 12 h. A piece of flesh lithium metal was used as the counter electrode. Celgard 2300 membrane was used as the separator and 1 M LiPF_6 solution in DMC/EC (1:1 in volume) was used as the electrolyte. The electrochemical characterization was carried out by galvanostatic cycling under different current densities between 1.0 and 2.5 V using a battery testing system (BTS-5V 10 mA, Neware). The electrochemical impedance spectrum (EIS) was tested using a 3-electrode device (ECC-Ref, EL-CELL) carried out on a Solartron impedance analyzer in a frequency range of 10^{-1} – 10^5 Hz. Impedance was measured at half state of the charge with a 5 mV ac perturbation.

3. Results and discussion

3.1. Structural and morphology characterizations

Fig. 1 shows the XRD patterns of glycerol assisted samples annealed at 500 °C (G-500) with a slightly difference in Ti:Li mole

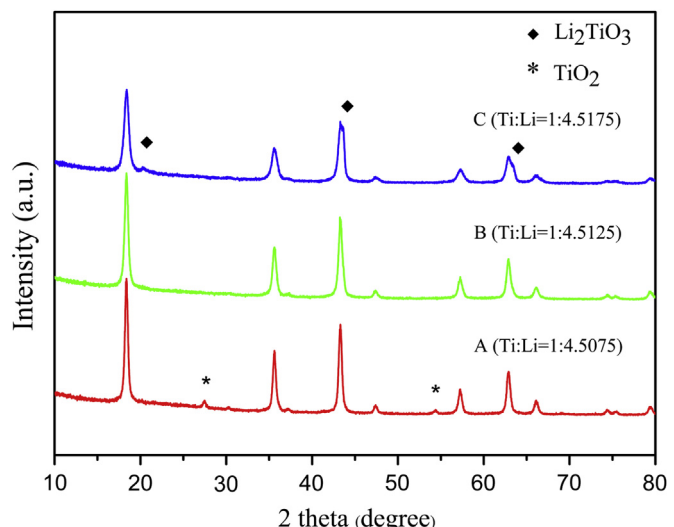


Fig. 1. XRD patterns for G-500 synthesized under different Ti:Li mole ratios.

ratio of starting materials. All the peaks can be indexed to $\text{Li}_4\text{Ti}_5\text{O}_{12}$ (JCPDS 49-0207) when the Ti:Li ratio of starting reactants is 1:4.5125 (sample B). But an impurity phase is observed with the slightly change in Ti:Li ratio. For sample A (Ti:Li = 1:4.5075), a trace of rutile TiO_2 impurity is obviously found at peaks of $2\theta = 27.4^\circ$, 54.3° . Similarly, peaks of $2\theta = 20.3^\circ$, 43.6° , 63.4° correspond to Li_2TiO_3 impurity for sample C (Ti:Li = 1:4.5175). It is suggested that the Ti:Li ratio of starting materials has a significant impact on the Ti:Li ratio of hydrothermal precursor and further affects the phase composition after subsequent calcination. Therefore, Ti:Li ratio of 1:4.5125 is applied for all the samples which are tested with further morphology investigation and electrochemical characterization in this experiment.

Fig. 2 shows the XRD patterns and TG-DSC curve of the hydrothermal precursor assisted by glycerol. The Ti:Li mole ratio used here is 1:4.5125. The XRD patterns in Fig. 2a are in accordance with a layered hydrous lithium titanate $\text{Li}_{1.81}\text{H}_{0.19}\text{Ti}_2\text{O}_5 \cdot 2\text{H}_2\text{O}$ (JCPDS 47–0123), which has been reported as the intermediate phase of hydrothermal process [17,32]. The TG-DSC curve in Fig. 2b reveals a total weight loss of around 25% for the hydrothermal precursor, which indicates that some free water and glycerol are absorbed in surface as the theoretical weight loss must be 18.2% according to formula of hydrous lithium titanate showed above. The weight loss below 150 °C is attributed to the desorption of surface free water and weight loss between 150 °C and 250 °C (about 15%) is mainly due to the loss of crystal water and combustion of absorbed glycerol. A strong exothermic peak at 306.8 °C can be assigned to the

transformation from the precursor to $\text{Li}_4\text{Ti}_5\text{O}_{12}$. The low transition temperature implies it is easy to obtain $\text{Li}_4\text{Ti}_5\text{O}_{12}$ from the hydrothermal precursor, which is consist with the result of previous work [32].

The hydrothermal precursor assisted by glycerol is annealed at 500 °C (G-500), 600 °C (G-600) and 700 °C (G-700) in air to investigate the influence of temperature. According to XRD patterns in Fig. 3, all the diffraction peaks of these samples are in accordance with cubic spinel $\text{Li}_4\text{Ti}_5\text{O}_{12}$. Obviously, the diffraction peaks gradually become sharper indicating an increase of crystallinity with the raising of calcination temperature. A sample without using glycerol annealed at 500 °C (S-500) is synthesized in order to study the influence of glycerol. The XRD patterns of S-500 can be indexed to spinel $\text{Li}_4\text{Ti}_5\text{O}_{12}$ as well.

The morphologies and sizes of as-prepared samples are investigated by SEM (Fig. 4) and TEM (Fig. 5). As can be seen from Fig. 4, the particle sizes for all samples are less than 100 nm. The S-500 (Fig. 4a) presents an irregular morphology, consisting of nanosheets, nanorods and plenty of nanoparticles. Fig. 4(b–d) displays the morphologies of glycerol assisted samples annealed at different temperature. It can be seen that the glycerol assisted samples have a cubic shape and the particle size is relatively uniform. The particle size gradually increases as the calcination temperature goes up. More detailed information can be found in the TEM images (Fig. 5). The hydrothermal precursor without glycerol (Fig. 5a) shows a jumble of substance. For S-500 °C (Fig. 5b), it displays an irregular morphology in which nanosheets, nanorods and nanoparticles can be found. The observations are in accordance with the SEM results in Fig. 4a. The hydrothermal precursor assisted by glycerol (Fig. 5c) is in a shape of cuboid with an average grain size of 15–20 nm. The HRTEM image inside Fig. 5c shows that interlayer spacing of hydrothermal precursor is 0.24 nm, corresponding to the (4 0 1) crystalline planes of $\text{Li}_{1.81}\text{H}_{0.19}\text{Ti}_2\text{O}_5 \cdot 2\text{H}_2\text{O}$. TEM images (Fig. 5d–f) for G-500, G-600, G-700 all display cubic shape and the particle size is quite uniform. The particle size is estimated to be approximately 25, 50, 80 nm for G-500, G-600 and G-700, respectively. The HRTEM image inside Fig. 5d shows that the interlayer spacing of G-500 is 0.48 nm, which is in accordance with the lattice spacing of (1 1 1) planes of $\text{Li}_4\text{Ti}_5\text{O}_{12}$.

BET analysis is carried out to obtain accurate information of the specific surface area. The experimental results are listed in Table 1.

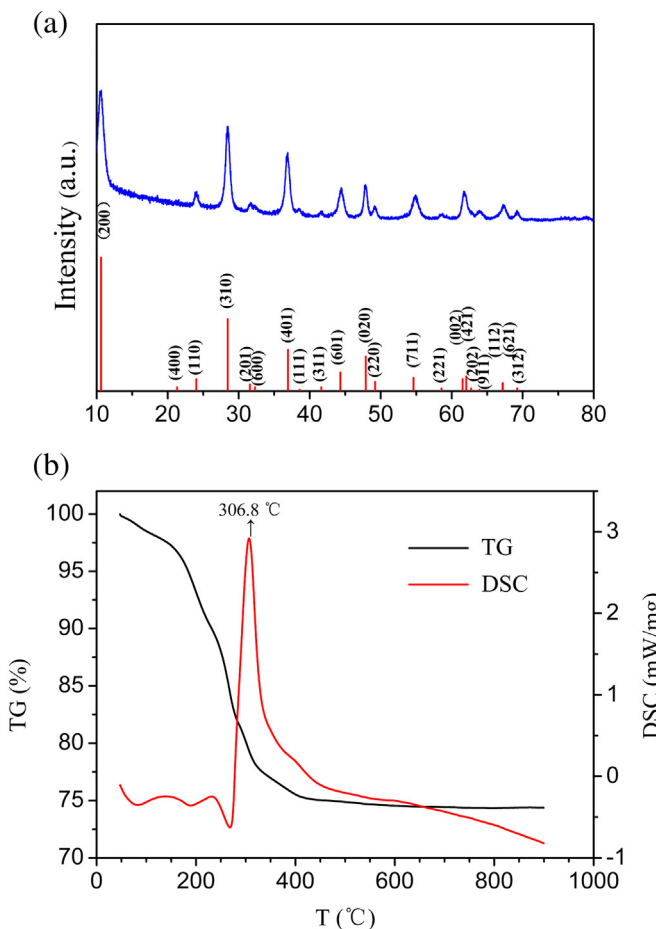


Fig. 2. XRD patterns (a) and TG-DSC curve (b) for hydrothermal precursor assisted by glycerol with a Ti:Li mole ratio of 1:4.5125.

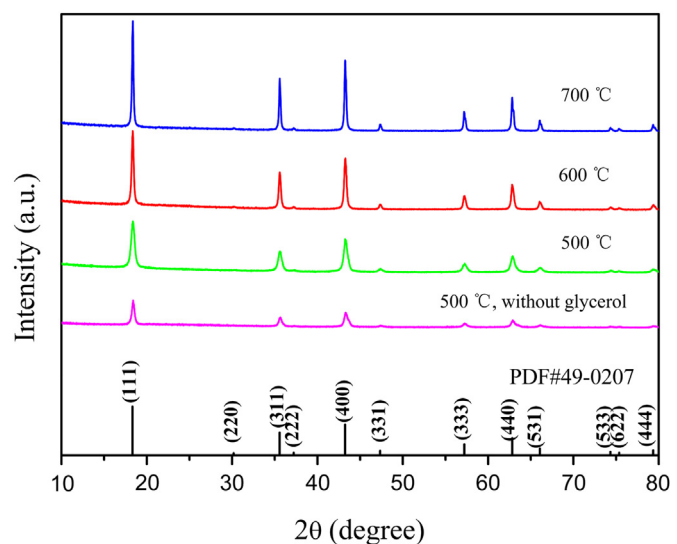


Fig. 3. XRD patterns for as-prepared $\text{Li}_4\text{Ti}_5\text{O}_{12}$: S-500, G-500, G-600 and G-700 synthesized under a Ti:Li mole ratio of 1:4.5125.

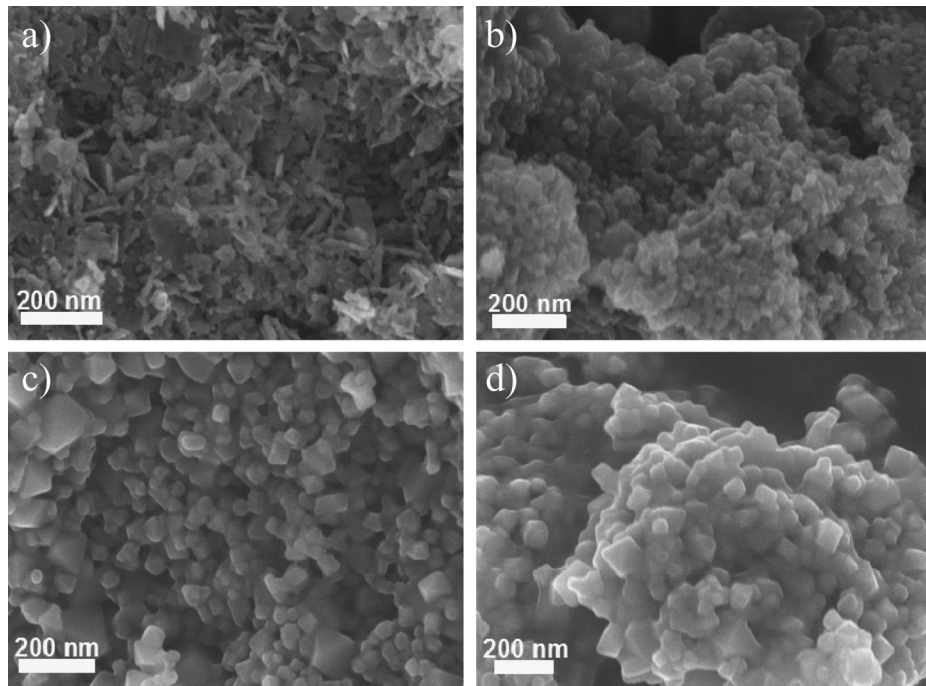


Fig. 4. SEM images for S-500 (a), G-500 (b), G-600 (c), G-700 (d).

For S-500, the measured specific surface area is $90.05 \text{ m}^2 \text{ g}^{-1}$. And for glycerol assisted samples, the specific surface areas are 85.93, 20.22 and $16.15 \text{ m}^2 \text{ g}^{-1}$ for G-500, G-600, G-700, respectively. S-500 has a slightly larger specific surface area compared with the samples assisted by glycerol, which is attributed to its special morphology which contains a variety of irregular nano-materials.

As mentioned above, pure nano- $\text{Li}_4\text{Ti}_5\text{O}_{12}$ is successfully synthesized by hydrothermal method. Nano-materials with a high specific area can offer better contacts with electrolytes and reduce the Li^+ diffusion distance. These two factors contribute to improve the rate capability of materials [33,34]. The introduction of glycerol here plays a special role. During the synthesis process, the solution goes through a transition process in morphology before hydrothermal treatment (see Fig. 6). Glycerol appears weak acidic property. It can coordinate with Ti^{4+} to a certain degree and effectively relieve the hydrolysis of Ti^{4+} . Along with the addition of LiOH , the pH of solution increases gradually. Meanwhile, Ti^{4+} starts to hydrolyze and forms a mass of flocculent precipitate. With the further addition of LiOH , the complexes react with more OH^- and become soluble because of the strong hydrogen bond interaction between the complexes and solvents. But for sample without glycerol, Ti^{4+} ions just react with OH^- and a large amount of precipitation like $\text{Ti}(\text{OH})_4$ or dehydration products of $\text{Ti}(\text{OH})_4$ are achieved in the end. Therefore, glycerol can help Ti^{4+} to be distributed uniformly in starting solution and conduce to form a cubic shape with a uniform particle size.

3.2. Electrochemical analysis

The electrochemical performances of as-prepared $\text{Li}_4\text{Ti}_5\text{O}_{12}$ are studied by galvanostatic method. Fig. 7a and b displays the charge and discharge profiles of G-500 and S-500 under different current density in the voltage range of 1–2.5 V. The charge/discharge rates vary from 0.1 C to 20 C. It can be found that G-500 exhibits larger capacity than S-500. The G-500 delivers a discharge capacity of 174 mAh g^{-1} at a low rate of 0.1 C, which is close to the theoretical capacity of $\text{Li}_4\text{Ti}_5\text{O}_{12}$ (175 mAh g^{-1}). However, the S-500 exhibits a

discharge capacity of 157 mAh g^{-1} at the same rate, which is approximately 17 mAh g^{-1} lower than G-500. The voltage plateau gap of charge/discharge profile is 0.025 V and 0.038 V for the two samples at 0.1 C rate. At higher charge/discharge rates, the G-500 delivers 170, 165, 161, 155 mAh g^{-1} at 1, 5, 10 and 20 C, while the corresponding value for S-500 is 152, 143, 140, 135 mAh g^{-1} , respectively. This indicates that the adding of glycerol in the synthesis process can effectively improve the rate performance of $\text{Li}_4\text{Ti}_5\text{O}_{12}$. It is worth noting that the G-500 exhibits a higher rate capability behavior which is superior to the performance reported for nanostructured $\text{Li}_4\text{Ti}_5\text{O}_{12}$ synthesized by hydrothermal method at similar rates [15,17].

Fig. 7c shows the rate performance of all calcined samples with the discharge rate from 1 C to 20 C. For each stage, the test is performed for 10 cycles. As shown in Fig. 7c, at 1 C and 5 C rate, the samples assisted by glycerol all exhibit better rate performance than S-500. The discharge capacity decreases as the rate increases, which is caused by the polarization. When the discharge rate increases to 10 C or 20 C, G-700 shows a rapid decay along with cycling. After 10 cycles at 20 C, the discharge capacity is 155, 148, 110, 135 mAh g^{-1} for G-500, G-600, G-700 and S-500, respectively. The G-500 and G-600 both exhibit excellent rate performance. The differences in electrochemical performance can be ascribed to disparities of their particle size and specific surface area.

The cycle performance of G-500 charged-discharged at 5 C is illustrated in Fig. 7d. An excellent cycle performance can be achieved with the sample. In the first 200 cycles, there is a gradually capacity attenuation. The initial discharge capacity is 165 mAh g^{-1} , but after 200 charge–discharge, the capacity remains at 156 mAh g^{-1} , which presents a 5.5% discharge capacity loss. After charge and discharge for 500 cycles, the capacity remains at 154 mAh g^{-1} and the capacity retention is 93.3%. It is worth noting that the total capacity loss is 6.7%, while the value is only 1.2% for the last 300 cycles.

To further understand the high rate performance of $\text{Li}_4\text{Ti}_5\text{O}_{12}$, electrochemical impedance spectrum (EIS) measurements are carried out at half state of charge for each sample (see Fig. 8). The Nyquist plot consists of a semicircle at high-to-medium frequency

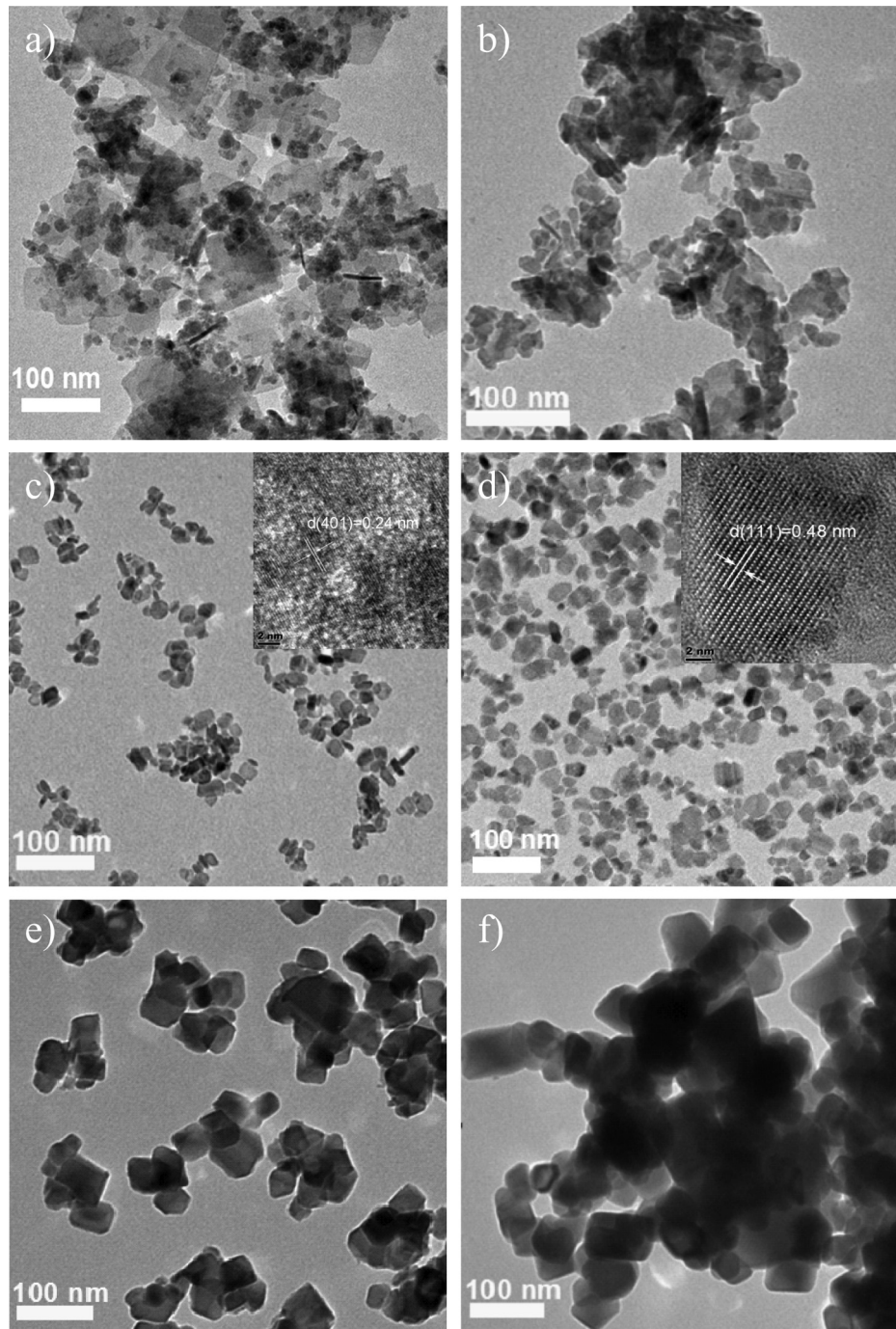


Fig. 5. TEM images for samples without glycerol: (a) hydrothermal precursor, (b) S-500; TEM images for samples assisted by glycerol: (c) hydrothermal precursor, (d) G-500, (e) G-600, (f) G-700.

region and a sloping line at low frequency region, which are referred to the charge-transfer reaction and Li^+ ion diffusion in the solid electrode material. The EIS is simulated using the equivalent circuit as shown in the inset of Fig. 8, in which R_s is the resistance of electrolyte, R_{ct} reflects the charge-transfer resistance and CPE stands for the double layer capacitance that takes the roughness of the particle surface into consideration [35]. The slope line corresponds to the Warburg impedance is represented by W_1 . The fitting results are listed in Table 2. It can be observed that G-500 shows the

Table 1
BET analysis results for each sample.

Samples	Specific surface area ($\text{m}^2 \text{ g}^{-1}$)	Mesoporous volume ($\text{cm}^3 \text{ g}^{-1}$)	Average pore size (nm)
S-500	90.05	0.41	8.3
G-500	85.93	0.36	6.0
G-600	20.22	0.13	13.3
G-700	16.15	0.11	14.2

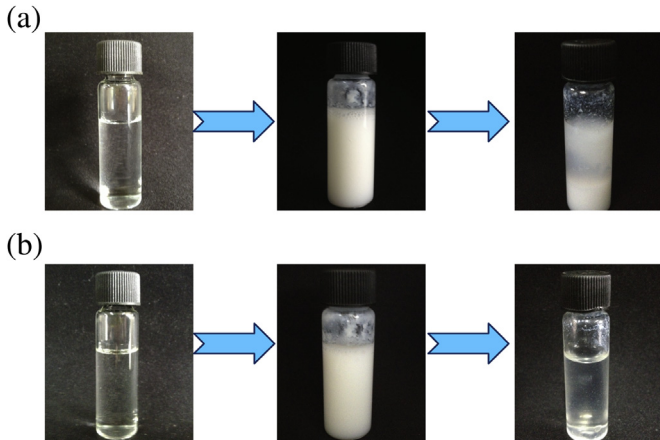


Fig. 6. Photos for solution state with adding different amounts of LiOH before hydrothermal treatment: (a) sample without glycerol, (b) sample assisted by glycerol. The amounts of LiOH added from left to right are none, half and fully.

lowest R_{ct} value (15.8Ω). This indicates that the sample has a better lithium ion transfer than the others. To further confirm this result, the lithium ion diffusion coefficient is calculated by the following Eq. (1) [36–38]:

$$D_{Li} = \frac{R^2 T^2}{2A^2 n^4 F^4 C^2 \sigma^2} \quad (1)$$

where D_{Li} represents the diffusion coefficient of the lithium ion, R is the gas constant, T is the absolute temperature, A is the surface area of electrode, n is the number of electrons per molecule during reaction, F is the Faraday constant, C is the concentration of lithium ion, and σ is the Warburg factor which can be calculated from Eq. (2):

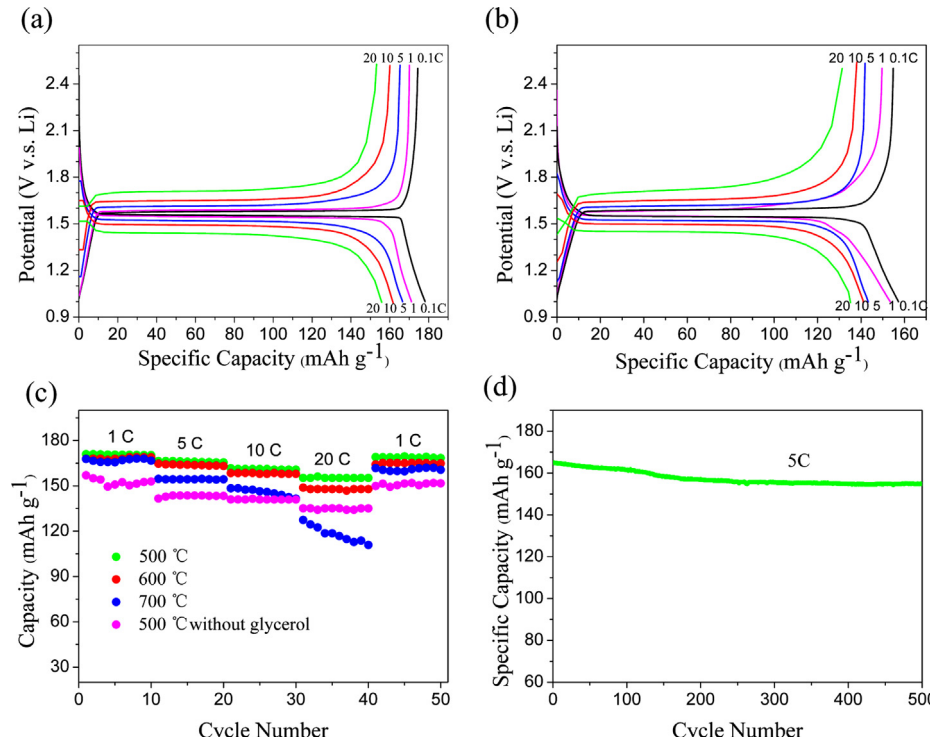


Fig. 7. Charge and discharge curves of S-500 (a) and G-500 (b) at the discharge rate from 0.1 C to 20 C; rate performance for all calcined samples (c) cycled from 1 C to 20 C and then to 1 C, each stage performed for 10 times; cycling performance of G-500 (d) at 5 C.

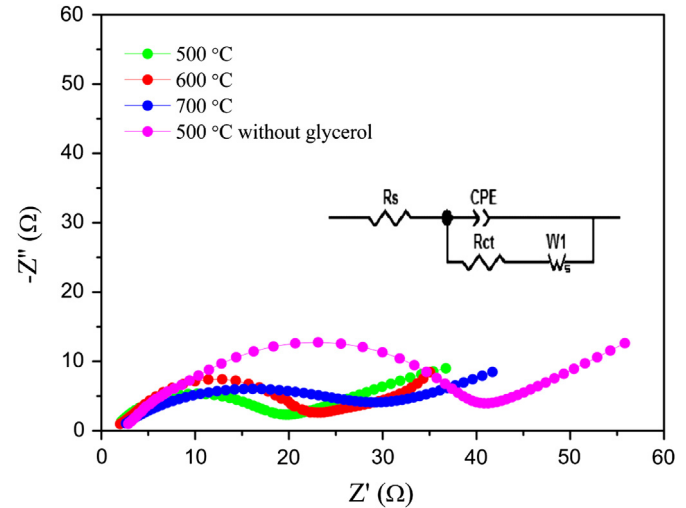


Fig. 8. Electrochemical impedance spectra of as-prepared $Li_4Ti_5O_{12}$ and an equivalent circuit as shown in the inset.

Table 2
Simulated results of the equivalent circuit for each sample.

Samples	R_s (Ω)	R_{ct} (Ω)	σ	D_{Li+} ($cm^2 s^{-1}$)
S-500	2.8	29.1	12.48	1.97×10^{-11}
G-500	2.1	15.8	8.42	4.32×10^{-11}
G-600	2.0	20.7	8.77	3.98×10^{-11}
G-700	2.6	26.1	9.71	3.25×10^{-11}

$$Z' = R_s + R_{ct} + \sigma \omega^{-1/2} \quad (2)$$

where Z' is real part of impedance, ω is the radial frequency, σ can be obtained from the slope of the fitted line between Z' and $\omega^{-1/2}$.

Calculated values can be seen from Table 2, G-500 exhibits the largest D_{Li} . The larger lithium ion diffusion coefficient means that a better capability to meet the lithium ion transfer at high charge/discharge rate.

4. Conclusion

In summary, we develop a facile approach to obtain pure nano- $Li_4Ti_5O_{12}$ by a glycerol assisted hydrothermal process. During the synthesis process, the Ti:Li ratio of starting materials has a closely influence on the final composition of product. A small deviation from the accurate ratio would lead to the formation of impurity phases (TiO_2 or Li_2TiO_3). The introduction of glycerol plays a crucial role in the synthesis process as well. For it helps to control the morphology of $Li_4Ti_5O_{12}$ and contributes to improve the electrochemical properties significantly. Considering the electrochemical properties, the G-500 exhibits the best electrochemical performance. It can deliver a discharge capacity of 174 mAh g^{-1} at a low rate of 0.1 C and reach a discharge capacity of 155 mAh g^{-1} even at a high rate of 20 C. The cycling performance is also exciting, the capacity can remain at 154 mAh g^{-1} and the capacity retention is 93.3% after 500 cycles at 5 C. The excellent rate and cycling performance is attributed to the minor particle size, smaller charge-transfer resistance (15.8Ω) and the larger lithium ion diffusion coefficient ($4.32 \times 10^{-11} \text{ cm}^2 \text{ s}^{-1}$). We believe that the nano- $Li_4Ti_5O_{12}$ synthesized by a glycerol assisted hydrothermal method could be a promising anode material for high rate lithium ion batteries.

Acknowledgments

The authors appreciate the financial support from State Key Basic Research Programme of PRC (2009CB220105, 2013CB934000), Beijing Natural Science Foundation (2120001), National Natural Science Foundation of China (21273129), Tsinghua University independent research program (20111081039), National International Science and Technology Cooperation Project (2012DFG61480), 863 (2011AA11A290) and China-US Electric Vehicle Project (2010DFA72760).

References

- [1] M. Armand, J.M. Tarascon, *Nature* 451 (2008) 652–657.
- [2] A.S. Aricò, P.G. Bruce, B. Scrosati, J.M. Tarascon, W. van Schalkwijk, *Nat. Mater.* 4 (2005) 366–377.
- [3] M. Tarascon, M.J. Armand, *Nature* 414 (2001) 359–367.
- [4] P.G. Bruce, B. Scrosati, J.M. Tarascon, *Angew. Chem. Int. Ed.* 47 (2008) 2930–2946.
- [5] X.L. Wu, L.Y. Jiang, F.F. Cao, Y.G. Guo, L.J. Wan, *Adv. Mater.* 21 (2009) 2710–2714.
- [6] H. Joachin, T.D. Kaun, K. Zaghib, J. Prakasha, *J. Electrochem. Soc.* 156 (2009) A401–A406.
- [7] Y.G. Wang, H.M. Liu, K.X. Wang, E.J. He, Y.R. Wang, H.S. Zhou, *J. Mater. Chem.* 19 (2009) 6789–6795.
- [8] B.K. Guo, J. Shu, K. Tang, Y. Bai, Z.X. Wang, L.Q. Chen, *J. Power Sources* 177 (2008) 205–210.
- [9] X. Li, H. Zhu, K. Wang, A. Cao, J. Wei, C. Li, Y. Jia, Z. Li, X. Li, D. Wu, *Adv. Mater.* 22 (2010) 2743–2748.
- [10] B. Markovsky, F. Amalraj, H.E. Gottlieb, Y. Gofer, S.K. Martha, D. Aurbach, *J. Electrochem. Soc.* 157 (2010) A423–A429.
- [11] F. Ronci, P. Reale, B. Scrosati, S. Panero, V.R. Albertini, M.D. Michiel, P. Perfetti, J.M. Merino, *J. Phys. Chem. B* 106 (2002) 3082–3086.
- [12] K. Ariyoshi, R. Yamato, T. Ohzuku, *Electrochim. Acta* 51 (2005) 1125–1129.
- [13] C.H. Chen, J.T. Vaughan, A.N. Jansen, D.W. Dees, A.J. Kahaian, T. Goacher, M.M. Thackeray, *J. Electrochem. Soc.* 148 (2001) A102–A104.
- [14] E.L. Kavan, J. Prochazka, T.M. Spitzer, M. Kalbac, M.T. Zukalova, T. Drezen, M. Gratzel, *J. Electrochim. Soc.* 150 (2003) A1000–A1007.
- [15] Y. Tang, L. Yang, S. Fang, Z. Qiu, *Electrochim. Acta* 54 (2009) 6244–6249.
- [16] L.F. Shen, C.Z. Yuan, H.J. Luo, X.G. Zhang, L. Chen, H.S. Li, *J. Mater. Chem.* 21 (2011) 14414–14416.
- [17] J.Z. Chen, L. Yang, S.H. Fang, Y.F. Tang, *Electrochim. Acta* 55 (2010) 6596–6600.
- [18] R. Xu, J.R. Li, A. Tan, Z.L. Tang, Z.T. Zhang, *J. Power Sources* 196 (2011) 2283–2288.
- [19] G.J. Wang, J. Gao, L.J. Fu, N.H. Zhao, Y.P. Wu, T. Takamura, *J. Power Sources* 174 (2007) 1109–1112.
- [20] H.Y. Yu, X.F. Zhang, A.F. Jalbout, X.D. Yan, X.M. Pan, H.M. Xie, R.S. Wang, *Electrochim. Acta* 53 (2008) 4200–4204.
- [21] Y.J. Hao, Q.Y. Lai, Z.H. Xu, X.Q. Liu, X.Y. Ji, *Solid State Ionics* 176 (2005) 1201–1206.
- [22] C.H. Jiang, M. Ichihara, I. Honma, H.S. Zhou, *Electrochim. Acta* 52 (2007) 6470–6475.
- [23] L.F. Shen, C.Z. Yuan, H.J. Luo, X.G. Zhang, K. Xua, Y.Y. Xia, *J. Mater. Chem.* 20 (2010) 6998–7004.
- [24] C. Lai, Y.Y. Dou, X. Li, X.P. Gao, *J. Power Sources* 195 (2010) 3676–3679.
- [25] L. Cheng, H.J. Liu, J.J. Zhang, H.M. Xiong, Y.Y. Xia, *J. Electrochim. Soc.* 153 (2006) A1472–A1477.
- [26] Y. Bai, F. Wang, F. Wu, C. Wu, L.Y. Bao, *Electrochim. Acta* 54 (2008) 322–327.
- [27] E. Matsui, Y. Abe, M. Senna, *J. Am. Ceram. Soc.* 91 (2008) 1522–1527.
- [28] T. Yuan, R. Cai, R. Ran, Y.K. Zhou, Z.P. Shao, *J. Alloys Compd.* 505 (2010) 367–373.
- [29] W.D. Shi, S.Y. Song, H.J. Zhang, *Chem. Soc. Rev.* (2013), <http://dx.doi.org/10.1039/C3CS60012B>.
- [30] J. Yang, C.X. Li, Z.W. Quan, C.M. Zhang, P.P. Yang, Y.Y. Li, C.C. Yu, J. Lin, *J. Phys. Chem. C* 112 (2008) 12777–12785.
- [31] L.X. Yang, Y.J. Zhu, L. Li, L. Zhang, H. Tong, W.W. Wang, G.F. Cheng, J.F. Zhu, *Eur. J. Inorg. Chem.* 23 (2006) 4787–4792.
- [32] M. Sugita, M. Tsuji, M. Abe, *Bull. Chem. Soc. Jpn.* 63 (1990) 1978–1984.
- [33] T. Djenizian, I. Hanzua, P. Knauth, *J. Mater. Chem.* 21 (2011) 9925–9937.
- [34] K.T. Lee, J. Cho, *Nano Today* 6 (2011) 28–41.
- [35] X. Li, M.Z. Qu, Y.G. Hua, Z.L. Yu, *Electrochim. Acta* 55 (2010) 2978–2982.
- [36] Y.H. Rho, K. Kanamura, *J. Solid State Chem.* 177 (2004) 2094–2100.
- [37] S.L. Chou, J.Z. Wang, H.K. Liu, S.X. Dou, *J. Phys. Chem. C* 115 (2011) 16220–16227.
- [38] B.H. Li, C.P. Han, Y.B. He, C. Yang, H.D. Du, Q.H. Yang, F.Y. Kang, *Energy Environ. Sci.* 5 (2012) 9595–9602.